American Journal of Condensed Matter Physics 2012, 2(5): 126-134
DOI: 10.5923/j.ajcmp.20120205.04

Structural and Electronic Properties Calculations of $AlAs_{1-x}P_x$ Alloy

Ali BENTOUAF*, Mohammed AMERI, Rezki MEBSOUT, Djelloul HACHEMANE

Département de Physique, Faculté des Sciences, Université Djillali LIABES, Sidi-Bel, Abbès, 22000, Algérie

Abstract Based on the self-consistent ab initio the full-potential linear muffin-tin orbital (FP-LMTO) method, the structural, electronic, optical, and thermodynamic properties of $AlAs_{1-x}P_x$ ternary semiconductor alloys have been investigated. The exchange–correlation potential was calculated using both the local density approximation (LDA) and generalized gradient approximation (GGA). The ground-state properties are determined for the cubic bulk materials AlAs, AlP, and their mixed crystals at various concentrations (x = 0.25, 0.5, and 0.75). Deviation of the lattice parameter from Vegard's law and the bulk modulus from linear concentration dependence has been examined. The microscopic origins of the band-gap bowing parameter have been discussed. Moreover, the refractive index for $AlAs_{1-x}P_x$ is studied using Reedy and Nazeer model. Besides, the thermodynamic stability of the alloys of interest is investigated by means of the miscibility critical temperature.

Keywords FP-LMTO, Electronic Properties, Optical Properties, $AlAs_{1-x}P_x$ Alloy

1. Introduction

Recently, III–V zinc blende semiconductors compounds have become an area of great technological activity. The reason for this is the possibility of producing novel materials with adjustable electronic and magnetic properties. Among them, the aluminum compounds AlAs and AlP are concerned in this paper. AlAs is one of the most important electronic and optoelectronic materials because of its frequent incorporation into GaAs-based heterostructures [1,2]. AlP, with the largest direct gap of the III–V compound semiconductors, is undoubtedly the most ''exotic'' and least studied[1]. However, in recent years, it is attracted special attention to its incorporation in the AlAs/AlP and GaP/AlP - based heterostructures. AlAs/AlP superlattices are attractive due to their potential applications in optoelectronic devices because they are expected to become direct band gap materials[3].

GaP/AlP-based heterostructures are attractive in their characteristics for the development of optoelectronic devices operating in the yellow-green spectral region[4,5] and are considered as an alternative to a GaN/AlGaN system for the development of infrared semiconductor lasers and detectors [6]. Although there have been numerous calculations[7–9] of the structural, electronic and optical properties of aluminum compounds using different methods, to our knowledge there are few reports that had used the full potential calculation FP-LAPW to calculate the electronic, structural and optical properties for those compounds. Khanin and Kulkova[10] and Reshak and Auluck[11] used FP-LAPW method within local density approximation (LDA)[12] of the exchange – correlation energy to calculate the electronic and optical properties respectively. Recently, Briki et al.[13] studied the effects of relativistic on the structural and transport properties of III–V compounds utilizing LDA and PBE-GGA [14] for the exchange– correlation energy.

In the present work, we have aimed to combine AlP and AlAs compounds having different structural and electronic properties in order to obtain new materials, $AlAs_{1-x}P_x$ ternary alloys with intermediate properties. However, to the best of our knowledge, no experimental or theoretical investigations of $AlAs_{1-x}P_x$ alloys have been appeared in the literature. The present work study the structural, electronic, optical, and thermodynamic properties of these alloys by using a full-potential, linear muffin-tin-orbital (FP-LMTO) method. The physical origins of gap bowing are calculated following the approach of Zunger and co-workers[15].

A brief description of the computational details and methodology are given in Section 2. We present the theoretical results and discussion concerning the structural, electronic, optical and thermodynamic properties in Section 3. The conclusion is given in Section 4.

2. Computational Details

The calculations reported here were carried out using the ab-initio full-potential linear muffin-tin orbital (FP- LMTO) method as implemented in the Lmtart code[16-18]. The

* Corresponding author:
lilo.btf@gmail.com (A. Bentouaf)
Published online at http://journal.sapub.org/ajcmp

exchange and correlation potential was calculated using the local density approximation (LDA)[19] and the generalized approximation (GGA)[20]. This is an improved method compared to previous (LMTO) methods. The FP-LMTO method treats muffin-tin spheres and interstitial regions on the same footing, leading to improvements in the precision of the eingen-values. At the same time, the FP-LMTO method, in which the space is divided into an interstitial regions (IR) and non overlapping muffin-tin spheres (MTS) surrounding the atomic sites, uses a more complete basis than its predecessors. In the IR regions, the basis functions are represented by Fourier series. Inside the MTS spheres, the basis functions are represented in terms of numerical solutions of the radial Schrödinger equation for the spherical part of the potential multiplied by spherical harmonics. The charge density and the potential are represented inside the MTS by spherical harmonics up to $l_{max} = 6$. The integrals over the Brillouin zone are performed up to 55 special k-points for binary com-pounds and 27 special k-points for the alloys in the irreducible Brillouin zone (IBZ), using the Blöchl's modified tetrahedron method[21]. The self - consistent calculations are considered to be converged when the total energy of the system is stable within 10^{-5} Ry. In order to avoid the overlap of atomic spheres the MTS radius for each atomic position is taken to be different for each case. Both the plane waves cut-off are varied to ensure the total energy convergence. The values of the sphere radii (MTS), number of plane waves (NPLW).

3. Results and Discussions

3.1. Structural Parameters

In this section the structural properties of the binary compounds AlAs and AlP were analyzed in the zinc blend structure. The alloys were modeled at some selected compositions x = 0.25, 0.5, 0.75 with ordered structures described in terms of periodically repeated supercells. For the considered structures, we perform the structural optimization by minimizing the total energy with respect to the cell parameters and also the atomic positions (as prototype, Table 1 summarizes the atomic positions for $AlAs_{1-x}P_x$). For the composition x = 0.25 and 0.75 the simplest structure is an eight-atom simple cubic lattice (luzonite): the anions with the lower concentration form a regular simple cubic lattice. For x = 0.5, the smallest ordered structure is a four-atom tetragonal cell, corresponding to the (0 0 1) superlattice. For the considered structures, the calculated total energy at many different volumes around equilibrium was fitted to the Murnaghan's equation of state[22] in order to obtain the equilibrium lattice constant and the bulk modulus for the binary compounds AlAs and AlP for different approximations of exchange–correlation energy GGA and LDA. The results of our calculations were summarized in Table 2 and were compared to other experimental and theoretical predictions.

The lattice constants obtained within the LDA for the parent binary system AlP and AlAs are respectively 0.38 % and 0.11 % lower than the experimental value, while the corresponding bulk modulus are 1.24% and 2.59% larger than the experimental value, which is the usual level of accuracy of the LDA. When comparing the results obtained within GGA, the lattice constant are 1.66 % for AlAs and 1.17 % for AlP larger than the experimental values and the corresponding bulk modulus are 20.38% and 4.77% smaller than the corresponding experimental values. Hence it is safe to conclude that the LDA bulk modulus and lattice constants is in fact in better agreement with the experimental data than the GGA values. The calculated bulks modulus using both approximation LDA and GGA decreases in going from AlP to AlAs, suggesting the more compressibility for AlP compared to that for AlAs.

Our GGA results of lattice constant and bulk modulus of AlAs and AlP show a good agreement with experiment and are more accurate than recent ones calculated by FP-LAPW within PBE-GGA[13]. The LDA and GGA of exchange – correlation energy have been employed to calculate the structural properties of $AlAs_{1-x}P_x$ alloys. The results are presented in Table 3.

In Fig. 1, we present our calculated lattice constants as a function of P concentration along with Vegard's law result. The lattice constant scales linearly with composition thus obeying Vegard's law[25]. Our results show a marginal upward bowing parameter equal to 0.00457 A° for LDA and 0.011 A° for GGA. Fig. 2 shows the bulk modulus as a function of concentration x for the alloys. A small deviation of the bulk modulus from the linear concentration dependence (LCD) with downward bowing equal to 4.026 GPa for LDA and 9.298 GPa for GGA is observed. The deviation from LCD should be mainly due to the bulk modulus mismatch between AlAs and AlP compounds. A more precise comparison for the behavior of the $AlAs_{1-x}P_x$ ternary alloys shows that a decrease of the lattice constant is accompanied by an increase of the bulk modulus. It represents bond strengthening or weakening effects induced by changing the composition.

Table 1. Atomic positions for $AlAs_{1-x}P_x$ alloys

x	Atom	Atomic position
0.25		
	Al	(1/4 1/4 1/4), (3/4 3/4 1/4), (3/4 1/4 3/4), (1/4 3/4 3/4)
	As	(0 1/2 1/2), (1/2 0 1/2), (1/2 1/2 0)
	P	(0 0 0)
0.5		
	Al	(1/4 1/4 1/4), (3/4 3/4 1/4), (3/4 1/4 3/4), (1/4 3/4 3/4)
	As	(0 1/2 1/2), (1/2 0 1/2)
	P	(0 0 0), (1/2 1/2 0)
0.75		
	Al	1/4 1/4 1/4), (3/4 3/4 1/4), (3/4 1/4 3/4), (1/4 3/4 3/4)
	As	(0 1/2 1/2)
	P	(0 0 0), (1/2 0 1/2), (1/2 1/2 0)

Table 2. The optimized lattice constant (a,A°), bulk modulus, (B, GPa), and first-order pressure derivative of bulk modulus (B_0) calculated by different exchange–correlation energy approximations for AlAs and AlP compounds. The other calculated and measured values are given for comparison

	Present work		*Other works*	
	LDA	***GGA***	***Theoretical***	***Experimental***
AlAs		5.754	5.74[a], 5.731[b], 5.726[b], 6.039[b]	
a	5.654	65.281	66.8[a], 67.732[b], 68.272[b], 48.96[b]	5.66c
B	70.133	3.602	4.47[a], 3.891[b], 3.851[b], 3.533[b]	82c
B′	3.727			-
AlP		5.534		
a	5.449	81.89	5.51[a], 5.511[b], 5.507[b], 5.745[b]	5.47c
B	87.067	2.88	82.5[a], 82.097[b], 82.619[b], 63.834[b]	86c
B′	2.704		4.11[a], 4.08[b], 4.054[b], 3.577[b]	-

[a]**Ref[13] :** M. Briki, M. Abdelouhaba, A. Zaoui, M. Ferhat, Superlatt. Microstruct. 45 (2009)80.
[b]**Ref[23] :** F. Annane, H. Meradji , S. Ghemid , F. El Haj Hassan, Computational Materials Science 50 (2010) 274–278.
[c]**Ref[24] :** K.-H. Hellwege, O. Madelung (Eds.), Semi-Conductor, Intrinsic Properties of Group IV Elements and III_V, II_VI and I_VII Compounds, Landolt-Bornstein New Series, Group III, vol. 22, Pt Springer, Berlin, 1982.

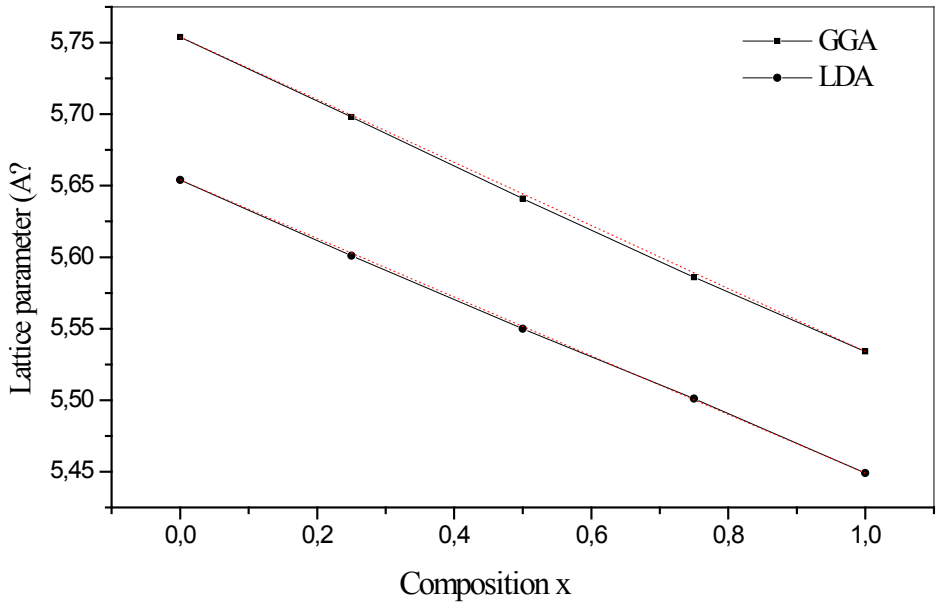

Figure 1. Composition dependence of the calculated lattice constants (solid squares) of GGA and (solid circle) of LDA of $AlAs_{1-x}P_x$ alloy compared with Vegard's prediction (dot line)

Table 3. Calculated band gaps for AlAs and AlP compounds along different line in k-space under LDA & GGA (all in eV)

Energy gap	Present work		Other works	
	LDA	GGA	Theoretical	Experimental
AlP				
(Γ- Γ)	3.366	3.088	2.94[a], 3.910[b], 3.083[b]	3.63[d]
(Γ- X)	1.465	1.638	1.54[a], 2.570[b], 1.632[b], 1.49[c]	2.52[d],2.5[e]
AlAs				
(Γ- Γ)	1.951	1.688	1.65[a], 2.486[b], 1.787[b]	3.13[d]
(Γ- X)	1.374	1.494	1.43[a], 2.349[b], 1.502[b], 1.39[c]	2.24[d],2.3[e]

[a]**Ref[13] :** M. Briki, M. Abdelouhaba, A. Zaoui, M. Ferhat, Superlatt. Microstruct. 45 (2009)80.
[b]**Ref[23] :** F. Annane, H. Meradji , S. Ghemid , F. El Haj Hassan, Computational Materials Science 50 (2010) 274–278.
[c]**Ref[11] :** Ali Hussain Reshak, S. Auluck, Physica B 395 (2007) 143.
[d]**Ref[26] :** M.P. Thompson, G.W. Auner, T.S. Zheleva, K.A. Jones, S.J. Simko, J.N. Hilfiker, J.Appl. Phys. 89 (2001) 3321.
[e]**Ref[7] :** (a) M.-Z. Huang, W.Y. Ching, Phys. Rev. B 47 (1993) 9449; (b) M.-Z. Huang, W.Y. Ching, Phys. Rev. B 47 (1993) 9464.

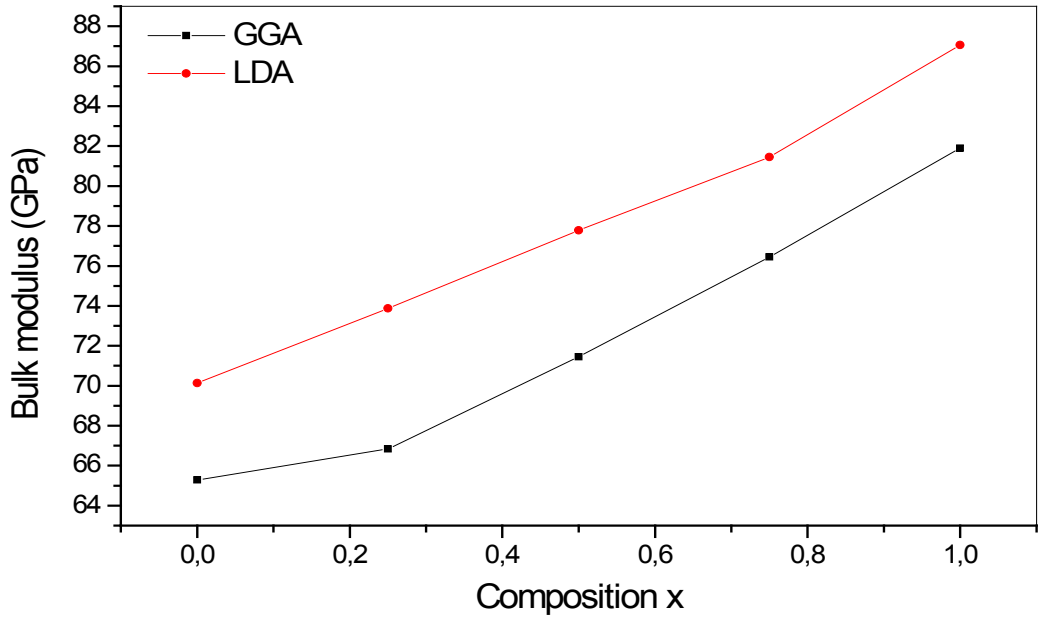

Figure 2. Composition dependence of the calculated bulk modulus (red solid) of LDA and (black solid) of GGA of $AlAs_{1-x}P_x$ alloy

3.2. Electronic Properties

The self consistent scalar relativistic band gaps of the compounds under investigation and their alloys were calculated within LDA and GGA schemes. An indirect band gap (Γ –X) has been observed for AlAs and AlP compounds. The results are presented in Table 3. The values obtained for the band gap within GGA are in better agreement with available experimental results in comparison with the values calculated by LDA. In fact, it is well known that the LDA usually underestimates the energy gap[27]. It is noticeable that the GGA scheme, which is based on potential optimization, is capable of giving a more reliable band structure. The calculated energy gaps for $AlAs_{1-x}P_x$ alloys are presented in Table 4. In Fig. 3, we display the composition dependence of the calculated band gaps using LDA and GGA schemes. The results are shown in Fig. 3 and obey the following variations:

$$E_g^{GGA}(x) = 1.498 + 0.220\,x - 0.081x^2 \quad (1)$$

$$E_g^{LDA}(x) = 1.377 + 0.138\,x - 0.052x^2 \quad (2)$$

Table 4. The concentration dependence of the lattice constants (a), bulk modulus (B), first order pressure derivatives of bulk modulus (B_0) and energy band gaps (Eg) calculated under GGA(LDA) schemes for $AlAs_{1-x}P_x$ alloys

x	a(A)	B(Gpa)	B'	Eg(eV)
AlAs	5.754(5.654)	65.281(70.133)	3.602(3.727)	1.494(1.374)
$AlAs_{0.75}P_{0.25}$				
Present work	5.698(5.601)	66.839(73.867)	3.445(3.664)	1.563(1.416)
Other works	5.672[a]	70.494[a]	4.093[a]	2.388[a],1.525[a]
$AlAs_{0.5}P_{0.5}$				
Present work	5.641(5.550)	71.456(77.778)	3.675	1.597(1.430)
Other works	5.618[a]	74.960[a]	4.036[a]	2.446[a],1.562[a]
$AlAs_{0.25}P_{0.75}$				
Present work	5.586(5.501)	76.455(81.454)	3.379(3.809)	1.624(1.448)
Other works	5.563[a]	78.445[a]	4.284[a]	2.513[a],1.599[a]
AlP	5.534(5.449)	81.89(87.067)	2.88(2.704)	1.638(1.465)

[a]**Ref[23] :** F. Annane, H. Meradji , S. Ghemid , F. El Haj Hassan, Computational Materials Science 50 (2010) 274–278.

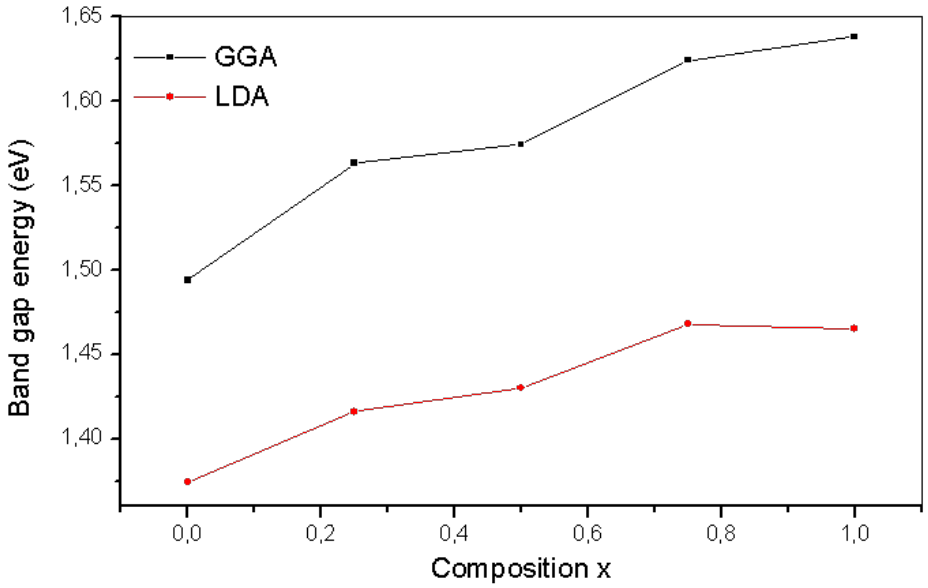

Figure 3. Variation of the calculated band gap versus x concentration of $AlAs_{1-x}P_x$ alloys using both GGA and LDA exchange and correlation potentials

From Fig. 3, it is clear that the alloys show a weakly compositional-dependent energy gap as conventionally known for III–V alloys[28]. In order to better understand the physical origins of the gap bowing parameter in $AlAs_{1-x}P_x$ alloys, we follow the procedure of Bernard and Zunger[15] and decompose the total bowing parameter b into physically distinct contributions. Since the compositional effect on the bowing is considered to be small, the band gap bowing equations of Bernard and Zunger have been defined only by the contributions of the volume deformation (b_{VD}), charge transfer (b_{CT}) and the structural relaxation (b_{SR}) of the alloys as follows:

$$b = b_{VD} + b_{CT} + b_{SR} \quad (3)$$

$$b_{VD} = 2[E_{AlAs}(a_{AlAs}) - E_{AlAs}(a) + E_{AlP}(a_{AlP}) - E_{AlP}(a)] \quad (4)$$

$$b_{CT} = 2[E_{AlAs}(a) + E_{AlP}(a) - 2E_{AlAsP}(a)] \quad (5)$$

$$b_{SR} = 4[E_{AlAsP}(a) - E_{AlAsP}(a_{eq})] \quad (6)$$

Here, a_{AlAs}, a_{AlP}, and a_{eq} are the equilibrium lattice constants of AlAs, AlP and $AlAs_{1-x}P_x$ alloys, respectively. The lattice constant (a) is calculated by linear composition dependence rule[25] for the alloys. All these energy gaps occurring in expressions (4)–(6) have been calculated for the indicated atomic structures and lattice constants. The calculated gap bowing contributions of the direct band gap are presented in Table 5. The total gap bowing for $AlAs_{1-x}P_x$ alloys has been found to be very small. The low value of b_{VD} is related to the weak mismatch of the lattice parameters of AlAs and AlP compounds and that of b_{CT} is due to the weak electronegativity[29] difference between As and P atoms. The small contribution of the structural relaxation to the bowing parameter it due to that our calculations are for ordered structure.

Table 5. Decomposition of optical bowing into VD, CT and SR contributions

Parameter	Present work		Other works
	LDA	GGA	
b_{VD}	0.082	0.072	-0.006[a],-0.01[a]
b_{CT}	4.826	3.089	0.064[a],0.038[a]
b_{SR}	0.005	0.009	-0.004[a],-0.008[a]
b	4.914	3.172	0.054[a],0.02[a],0.051[a],0.023[a]

[a]**Ref[23] :** F. Annane, H. Meradji , S. Ghemid , F. El Haj Hassan, Computational Materials Science 50 (2010) 274–278.

3.3. Linear Optical Properties

It is well known that the basic optical properties of semiconductors result from the electronic excitation in crystals when an electromagnetic wave is incident on them. The calculation of the optical properties of the solids is beset with numerous problems. The knowledge of the dielectric functions $\varepsilon(\omega) = \varepsilon_1(\omega) + i\varepsilon_2(\omega)$ allows to describe the optical properties of the medium at all phonon energies. Calculations of the dielectric function involve the energy eigen-values and the electron wave functions. These are the natural output of the *ab initio* band structure calculation which is usually performed under LDA and GGA[30,31] .We have calculated the frequency dependent imaginary dielectric function and real dielectric function. The effects of using *K* points in the BZ have already been discussed in the earlier work by Khan *et al* (1993)[32]. The knowledge of both the real and the imaginary parts of the dielectric function allows the calculation of important optical functions. In this paper, we also present and analyze the refractive index $\varepsilon(\omega)$ given by:

$$n(\omega) = \left[\frac{\varepsilon_1(\omega)}{2} + \frac{\sqrt{\varepsilon_1^2(\omega)+\varepsilon_2^2(\omega)}}{2}\right]^{1/2} \quad (7)$$

At low frequency ($\omega = 0$), we obtain the following relation:

$$n(0) = \varepsilon^{\frac{1}{2}}(0) \quad (8)$$

The refractive index and dielectric constants are very important to determine the optical and electric properties of the crystal. Advanced applications of these alloys can significantly benefit from accurate index data. The use of fast non-destructive optical techniques for epitaxial layer characterization (determination of thickness or alloy composition) is limited by the accuracy with which refractive indices can be related to alloy composition. These applications require an analytical expression or known accuracy to relate the wavelength dependence of refractive index to alloy composition, as determined from simple techniques as photoluminescence. Different theoretical models relate the refractive index to the energy band gap for a large set of semiconductors[33–36]. Especially, for the III–V semiconductors and its alloys we take the most realistic model, proposed by Reedy and Nazeer Ahammed[36]:

$$n = \sqrt{\frac{12.417}{\sqrt{E_g - 0.365}}} \quad (9)$$

where E_g is the energy gap in eV. This equation is a straightforward modification of the original Moss equation[34], with a second arbitrary constant (0.365) added in order to improve the results obtained.

In Table 6, we summarize the calculated values of the refractive index for the alloy under investigation, obtained by using the FP-LMTO method and Reddy et al. model. Comparison with the available data has been made where possible. It is clear that the values of the refractive index obtained by the FP-LMTO occur within the range of those obtained using Reddy et al. model; and for the end-point compounds (i.e. AlAs and AlP) are in good agreement with available experimental results.

Fig. 4 shows the variation of the calculated refractive index versus concentration for the alloys. One can notice that the refractive index decreases monotonically with increasing P content over the entire range of 0–1 for both FP-LMTO and model used. The calculated refractive index versus concentration is fitted by a polynomial equation. The results are summarized as follows:

$$n(x) = 2.271 - 0.186\,x - 0.024x^2 \quad \textit{FP-LMTO (LDA)} \quad (10)$$

$$n(x) = 2.324 - 0.449\,x - 0251\,x^2 \quad \textit{FP-LMTO (GGA)} \quad (11)$$

$$n(x) = 3.512 + 0.116\,x - 0.045x^2 \quad \textit{Reddy et al.(LDA)} \quad (12)$$

$$n(x) = 3.414 - 0.161\,x + 0.064x^2 \quad \textit{Reddy et al.(GGA)} \quad (13)$$

From these equations, we can note the weak non-linear dependence of the refractive index of the alloys with concentration x. Interestingly, we note on going from AlAs to AlP the band gap of $AlAs_{1-x}P_x$ increases (see Fig. 3) but the refractive index decreases. This is in agreement with the quantum-mechanics equation *(n(Eg))*[38] which states that when the band gap *Eg* increases, the refractive index n decreases, and vice versa, but not linearly.

Table 6. Refractive index of $AlAs_{1-x}P_x$ alloys for different compositions x

	Present work *FP-LMTO*		*Reedy model*		*Other works* *Theoretical*	
	LDA	*GGA*	*LDA*	*GGA*		*Experimental*
AlAs	2.276	2.330	3.515	3.418	2.833[a], 2.969[a]	3.00[b]
$AlAs_{0.75}P_{0.25}$	2.218	2.216	3.480	3.368	2.757[a],2.955[a]	-
$AlAs_{0.5}P_{0.5}$	2.186	2.160	3.468	3.360	2.715[a],2.934[a]	-
$AlAs_{0.25}P_{0.75}$	2.153	2.142	3.454	3.326	2.671[a],2.911[a]	-
AlP	2.106	2.119	3.440	3.317	2.651[a],2.892[a]	2.75[b]

[a]**Ref[23] :** F. Annane, H. Meradji , S. Ghemid , F. El Haj Hassan, Computational Materials Science 50 (2010) 274–278.
[b]**Ref[37] :** R.R. Reedy et al., J. Alloys Compd. 473 (2009) 28.

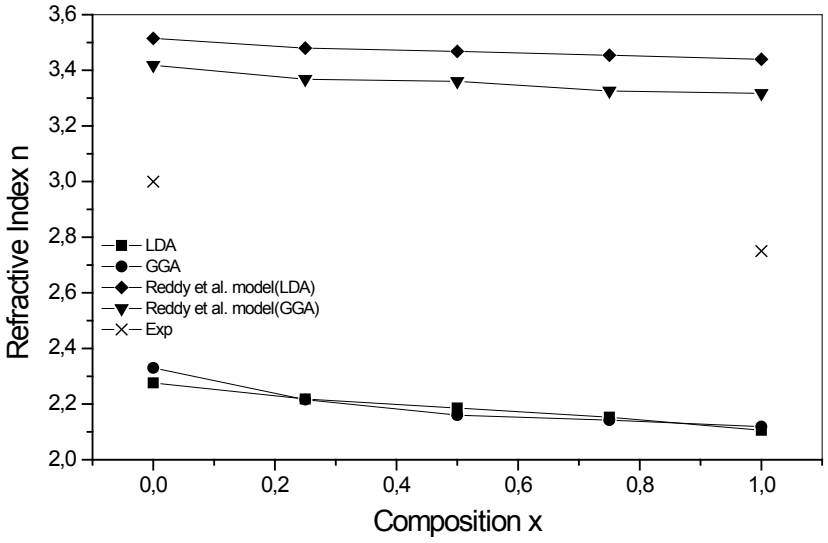

Figure 4. Variation of the calculated refractive index versus x concentration of $AlAs_{1-x}P_x$ alloys using both GGA and LDA exchange and correlation potentials

3.4. Thermodynamic Properties

In this section we present a rigorous theoretical study of the thermodynamic properties of $AlAs_{1-x}P_x$ alloys, the calculations carried out here are based on ab initio method within GGA scheme. We calculate the Gibbs free energy of mixing ΔG_m *(x, T)* which allows us to access the *T–x* phase diagram and obtain the critical temperature, Tc, for miscibility. Details of the calculations are given in Refs.[39–41]. For alloys, Gibbs free energy of mixing ΔG_m is expressed as:

$$\Delta G_m = \Delta H_m - T\Delta S_m \quad (14)$$

where

$$\Delta H_m = \Omega x(1-x) \quad (15)$$

$$\Delta S_m = -R[x\,lnx + (1-x)\ln(1-x)] \quad (16)$$

ΔH_m and ΔS_m are the enthalpy and entropy of mixing, respectively; Ω the interaction parameter and depends on material; *R* the gas constant and *T* the absolute temperature.

Indeed, an importance contribution arises from the mixing enthalpy, which can be obtained from the calculated total energies as $\Delta H_m = E_{AlAs\,1-xPx} - (1-x)E_{AlAs} - xE_{AlP}$, where $E_{AlAs\,1-xPx}$, E_{AlAs} and E_{AlP} are the respective energies of $AlAs_{1-x}P_x$ alloy, and the binary compounds AlAs and AlP. We then calculated ΔH_m to obtain Ω as a function of concentration. From a linear fit we obtained:

$$\Omega(Kcal/mol) = 4.566 - 2.721x$$

which shows the marginal dependence of Ω to the concentration x for $AlAs_{1-x}P_x$ alloys.

Now, we first calculate ΔG_m by using Eqs. (14)–(16). Then we use the Gibbs free energy at different concentrations to calculate the *T–x* phase diagram which shows the stable, metastable and unstable mixing regions of the alloy. At a temperature lower than the critical temperature *Tc*, the two binodal points are determined as those points at which the common tangent line touches the ΔG_m curves. The two spinodal points are determined as those points at which the second derivative of ΔG_m is zero; $\partial^2(\Delta G_m)/\partial x^2 = 0$.

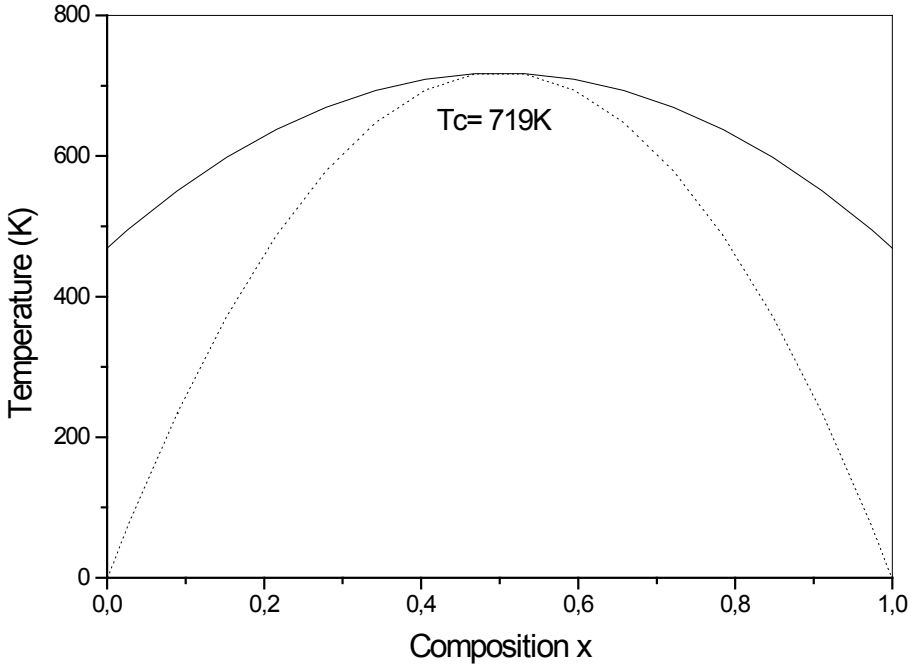

Figure 5. T–x phase diagram for $AlAs_{1-x}P_x$ alloys. Dotted line: binodal curve; solid line: spinodal curve

Fig. 5 shows the calculated phase diagram including the spinodal and binodal curves for the alloy of interest. We have calculated the phase diagram by using the average value of the x-dependent Ω, hence the phase diagram looks symmetric. We observed a critical temperature *Tc* of 719K for $AlAs_{1-x}P_x$ alloys. The spinodal curve in the phase diagram marks the equilibrium solubility limit, i.e. the miscibility gap. For temperatures and compositions above this curve a homogeneous alloy is predicted. The wide range between spinodal and binodal curves indicates that the alloy may exist as a metastable phase. Hence our results indicate that the $AlAs_{1-x}P_x$ alloys are stable at relatively high temperature.

4. Conclusions

In this paper, the structural, electronic, optical and thermodynamic properties of the zinc blend $AlAs_{1-x}P_x$ ternary alloys as a function of the composition x are presented using density-functional theory within different approximations of exchange-correlation energy: LDA and GGA. A nonlinear behavior of the lattice constant, bulk modulus and band gap dependence on x has been observed. Our results are in favorable agreement with the previous theoretical works. The bowing is found to be mainly caused by the charge transfer effect, while the volume deformation and the structural relaxation contribute to the bowing parameter at smaller magnitude.

We find that n(Eg) for $AlAs_{1-x}P_x$ alloys increases with decreasing energy gap, in agreement with the quantum-mechanics equation. The investigation of the thermodynamic stability allowed us to calculate the critical temperature which is 719K.

REFERENCES

[1] I. Vurgaftman, J.R. Meyer, L.R. Ram-Mohan, J. Appl. Phys. 89 (2001) 5815.

[2] S. Adachi, GaAs and Related Materials: Bulk Semiconducting and Superlattice Properties, World Scientific, Singapore, 1994.

[3] T. Ohnuma, M. Nagano, Jpn. J. Appl. Phys. 39 (2000) L972.

[4] A. Morii, H. Okagawa, K. Hara, et al., Electron. Lett. 28 (1992) 836.

[5] R.K. Soni, S. Tripathy, H. Asahi, Physica E 21 (2004) 131.

[6] M.P. Semtsiv, U. Müller, W.T. Masselink, et al., Appl. Phys. Lett. 89 (2006) 84102.

[7] (a) M.-Z. Huang, W.Y. Ching, Phys. Rev. B 47 (1993) 9449; (b) M.-Z. Huang, W.Y. Ching, Phys. Rev. B 47 (1993) 9464.

[8] A.R. Jivani, H.J. Trivedi, P.N. Gajjar, A.R. Jani, Pramana J. Phys. 64 (1) (2005) 153.

[9] S.Zh. Karaahanov, L.C. Yan Voon, Semiconductors 39 (2) (2005) 161.

[10] D.V. Khanin, S.E. Kulkova, Russ. Phys. J. 48 (1) (2005) 70.

[11] Ali Hussain Reshak, S. Auluck, Physica B 395 (2007) 143.

[12] J.P. Perdew, Y. Wang, Phys. Rev. B 45 (1992) 13244.

[13] M. Briki, M. Abdelouhaba, A. Zaoui, M. Ferhat, Superlatt. Microstruct. 45 (2009) 80.

[14] J.P. Perdew, S. Burke, M. Ernzerhof, Phys. Rev. Lett. 77 (1996) 3865.

[15] (a) G.P. Srivastava, G.L. Martins, A. Zunger, Phys. Rev. B 31 (1985) 2561; (b) J.E. Bernard, A. Zunger, Phys. Rev. B 34 (1986) 5992.

[16] S. Y. Savrasov, Phys. Rev. B 54 , (1996) 16470

[17] S. Savrasov, D. Savrasov, Phys. Rev. B 46 (1992) 12181

[18] D. Rached, M. Rabah, N. Benkhettou, M. Driz and B. Soudini Physica B : Physics of Condensed Matter, 337/1-4 (2003) pp. 394-403

[19] J.P. Perdew, Y. Wang, Phys. Rev. B 45 (1992) 13244.

[20] J.P. Perdew, S. Burke, M. Ernzerhof, Phys. Rev. Lett. 77 (1996) 3865

[21] P. Blochl, O. Jepsen, and O. K. Andersen, Phys. Rev. B 49, 16223 (1994).

[22] F.D. Murnaghan, Proc. Nat. Acad. Sci. USA 30 (1944) 5390.

[23] F. Annane, H. Meradji , S. Ghemid , F. El Haj Hassan, Computational Materials Science 50 (2010) 274–278.

[24] K.-H. Hellwege, O. Madelung (Eds.), Semi-Conductor, Intrinsic Properties of Group IV Elements and III_V, II_VI and I_VII Compounds, Landolt-Bornstein New Series, Group III, vol. 22, Pt Springer, Berlin, 1982

[25] L. Vegard, Z. Phys. 5 (1921) 17.

[26] M.P. Thompson, G.W. Auner, T.S. Zheleva, K.A. Jones, S.J. Simko, J.N. Hilfiker, J.Appl. Phys. 89 (2001) 3321.

[27] P. Dufek, P. Blaha, K. Schwarz, Phys. Rev. B 50 (1994) 7279.

[28] F. El Haj Hassan, H. Akbarzadeh, Mater. Sci. Eng. B 121 (2005) 170.

[29] W. Sargent, Table of Periodic Properties of the Elements, Sargent-Welch Scientific, Skokie, IL, 1980.

[30] Alouani M, Koch J M and Khan M A J. Phys. F16 (1986) 437

[31] Koenig C and Khan M A Phys. Rev. B17 (1983) 6129

[32] Khan M A, Kashyap A, Solanki A K, Nautiyal T and Auluck S Phys. Rev. B48 (1993)16947

[33] Y. Al Douri, H. Abid, H. Aourag, Mater. Chem. Phys. 65 (2000) 117.

[34] T.S. Moss, Phys. Status Solidi (b) 131 (1985) 415.

[35] N.M. Ravindra, S. Anuch, V.K. Srinvastava, Phys. State Solid (b) 93 (1979) 115.

[36] R. Reddy, Y. Nazeer Ahammed, Infra. Phys. Technol. 36 (1995) 825.

[37] R.R. Reedy et al., J. Alloys Compd. 473 (2009) 28.

[38] M. Anani, C. Mathieu, S. Lebida, Y. Amar, Z. Chama, H. Abid, Comput. Mater. Sci. 41 (2008) 570.

[39] R.A. Swalin, Thermodynamics of Solids, Wiley, New York, 1961.

[40] L.G. Ferreira, S.H. Wei, J.E. Bernard, A. Zunger Phys. Rev. B 40 (1989) 3197.

[41] L.K. Teles, J. Furthmüller, L.M.R. Scolfaro, J.R. Leite, F. Bechstedt, Phys. Rev. B 62(2000) 2475